

Chapter

HYDROXYAPATITE FORMATION ON METALLURGICAL GRADE POROUS SILICON NANOSPONGE PARTICLES

***E. G. Chadwick^{1,2}, O. M. Clarkin³
and D. A. Tanner^{1,2,*}***

¹Materials and Surface Science Institute,

²Department of Design and Manufacturing Technology,
University of Limerick, Ireland

³School of Mechanical and Manufacturing Engineering,
Dublin City University, Ireland

ABSTRACT

Investigations into the development of potential bone substitutes have increased rapidly in the last decade. Titanium and cobalt chrome are currently the alloys of choice when it comes to the orthopedic medical device fields due to their excellent mechanical strength and corrosion-resistant properties. Yet these materials are unable to elicit a biologically functional bone-material interface without a bioactive surface coating or surface modification. Osteoconductivity is only achieved when suitable coatings are applied or their surface properties are suitably altered. The need for significant bony reconstruction implants as a result of prosthetic

* E-mail: david.tanner@ul.ie, Tel: 00-353-(0)61-234130; Fax: 00-353-(0)61-202913.

revision surgery also increases the need to produce longer lasting or permanent bone substitute materials.

Hydroxyapatite is the principle constituent of bone and has been used as a mechanism to induce bone formation at particular biological sites in need of bone repair and growth. When applied as a surface coating, hydroxyapatite's chemical and physical properties allow osteointegration of medical devices and prostheses. The discovery of hydroxyapatite has resulted, not only in rapid advances and developments in the orthopedic and dental fields, but has also lead to a surge in investigations into further tailoring of the material to create new devices that meet clinical needs. Currently, the most commonly used method for assessing the potential bioactivity and bone-bonding ability of a material *in-vitro* involves using simulated body fluid. Previous research by Kokubo *et al.* has shown that *in-vitro* results obtained using these experiments correlate directly to *in-vivo* results and thus satisfies their use as potential bone-tissue substitutes.

Porous silicon is a bioactive material and has been the subject of intense research since its original discovery at the Bell labs in 1956. Canham *et al.* was the first to suggest the possibility of creating biologically interfaced devices from porous silicon given its biostability, non-toxicity and ease of its topographical manipulation and optoelectronic properties. Porous silicon has been shown to induce the formation of a physiologically stable hydroxyapatite on its surface using *in-vitro* simulated body fluid experiments. Other studies today are also exploring the use of porous silicon as a promising potential bioactive therapeutic agent and drug delivery vehicle. Further research exploring the potential of using a silicon-substituted hydroxyapatite coating in *in-vitro* experiments have showed improved bioactivity and chemical stability under physiological conditions compared to normal hydroxyapatite. In 2010, Chadwick, Clarkin and Tanner showed that metallurgical grade porous silicon powder induced bone-like apatite formation on its surface in simulated body fluid inferring a bioactive nature and likely close bony apposition *in-vivo*. This chapter explores the use of porous silicon as a biomaterial and hydroxyapatite and porous silicon as a potential biomaterial for bone tissue engineering and other bioactive applications. It examines current research and future directions of such biomaterials.

INTRODUCTION

From a biological perspective Si is an essential trace element which has been linked to the health of connective tissues and bones [1]. Previous research investigating the role of Si within the body has shown that increased

dietary Si is associated with increased bone mineral density (BMD) in the cortical hip bone of a range of subjects [2]. Large differences were observed in BMD values (up to 10%) for a dietary intake of between the greater than 40mg Si/day and the less than 14 mg Si/day quintiles of Si intake.

The range of subjects included 1295 men (aged 59.4 +/- 9.6 years), 306 premenopausal women (aged 47.0 +/- 4.7 years) and 1325 postmenopausal women (aged 61.4 +/- 8.3 years). Dietary Si was obtained from food sources such as cereals/grains and their products such as breakfast cereals, bread, beer, and some fruits and vegetables such as bananas, beans and lentils [2]. This research shows that Si can be used to stimulate bone growth through an increased dietary or supplement intake. The average dietary intake currently for Si is between 20-50mg Si/day in the Western world [2]. Carlisle *et al.* first reported the presence of Si (0.5 wt%) *in-vivo* within the mineral osteoid regions such as the active calcification sites of normal tibia from young mice and rats [3].

It was also demonstrated that Si supplemented embryonic chick bones showed a 100% increase in collagen content over Si-low bones after 12 days in culture [4]. Studies of skeletal development in Si-depleted chicks showed reduced circumference of leg bones with a thinner cortex and reduced flexibility [5].

Hydroxyapatite (HA), is a biomimetic calcium phosphate (CaP) ceramic with a similar composition to bone mineral [6]. It is bioactive and has been therefore used in dental and medical applications including coatings for hip replacements and bone grafting materials for filling bone cavities [6]. Silicon, when substituted into HA has been shown to improve bioactivity and increase the bone bonding ability of the ceramic (see Table 1).

Carlisle *et al.* has shown that Si is concentrated in the active bone growth sites of young mice and rats (co-localized with osteoblasts) and increased together with the level of Ca in osteoid tissues [5].

Table 1. Comparison of *in-vitro* and *in-vivo* bioactivity of HA and Si-HA [7-8]

	HA	0.8 wt. %	1.6 wt. %
Time required to form a surface layer of apatite <i>in-vitro</i> (days)	24	17	11
Percentage bone/implant coverage at 23 days <i>in-vivo</i>	47.1%±3.6	59.8%±7.3	-

As the bones develop or ‘mature’, the Si levels diminish as Ca levels increase to those of fully mineralized bone. This research suggests that Si may have a role in the development of an organic matrix and subsequent initiation of calcification and is further evidenced by the concentrations of collagen and glycosaminoglycins which are suppressed in Si deficient animals while the mineral composition of bone is largely unaffected [5]. Glycosaminoglycins are shown to be associated with Si in numerous tissue types and it has been indicated that Si is associated with organic phosphorus prior to calcification [5].

These results support the arguments that Si has a role in co-coordinating glycoprotein phosphorylation reactions with collagen prior to the growth of HA crystals [5].

POROUS MATERIALS

Porous materials can be defined as any solid material containing pores [9]. The porosity of a material generally means the fraction of pore volume to the total volume of the material. It consists of individual openings, spacings or interconnecting pores [9].

Porosity can occur at a substrate surface or can completely penetrate through a bulk material [10]. According to the IUPAC (International Union of Pure and Applied Chemistry), porous materials are divided into three categories: microporous or nanoporous (<2nm), mesoporous (2-50 nm) and macroporous (>50nm) [11].

Pores within a material are classified into two types: open pores and closed pores [9]. The open pores connect to the outside of the material whilst the closed pores are isolated from the outside and may contain a fluid. Most of the industrial applications today require porous material with open pores.

Porous materials for filters and carriers for catalysts and bioreactors need to have a high fraction of open porosity. Closed porous materials are used mainly for sonic and thermal insulators or low-specific-gravity structural components [9].

Nano-porous materials abound in nature both in biological systems and in natural minerals. Bulk nano-porous materials which can be visualised as diminutive sponge-like substances, are gaining increasing importance in industrial applications such as molecular sieving, ion exchange and catalysis [12].

POROUS SILICON

Porous silicon (PS) is considered a sponge-like structure created by either electro-chemical or chemical etching of bulk silicon [13]. This produces a random array of pores within the silicon material. PS was originally discovered by Arthur Uhlir Jr. and his wife Ingeborg, at the Bell laboratories in the US between 1955 and 1956 [14]. Uhlir and Ingeborg were developing a technique for cleaning, polishing and shaping the surfaces of germanium and silicon by electrochemical etching in hydrofluoric (HF) acid solutions [14]. Uhlir discovered that low current densities would induce a red or black crude product in the form of a thick film on the surface of the material. In 1971, Watanabe and Sakai demonstrated the first application of PS in electronics with 'full isolation by the porous oxidized process' (FIPOS), where the PS layers were used for device isolation in integrated circuits [15]. The main focus of research during this period was based on using oxidised porous silicon as a dielectric isolator [14]. Then, in the late 1980's, at the Defence Research Agency in England, Leigh Canham discovered that PS was able to display quantum confinement effects. In a published experiment in 1990 it was revealed that silicon wafers can emit light if subjected to electrochemical and chemical dissolution [16]. This particular phenomenon is known as photoluminescence. Major interest has since grown concerning the uses and various applications that could arise from using PS [16].

POROUS SILICON FORMATION

The two most commonly employed methods applied to achieve PS formation are electro-chemical etching and chemical etching of Si in HF based solutions [17-18]. In the case of electrochemical etching of pure intrinsic Si wafers, it is generally accepted that only a hydrogen (H) passivated surface layer results [19]. Hole injection and doping in bulk Si wafers prior to etching is essential to allow the HF electrolyte penetrate into voids and attack the material thereby resulting in the initial dissolution phase of the Si surface layer and a porous surface structure being formed [19]. The anodisation cell can be one of three types such as a lateral cell, single-tank or double tank cell and the potential current applied, usually a constant current at low current density, allows maximum control of parameters such as porosity, thickness and uniformity of the final PS layer structure [20]. Pore initiation and dissolution

in the Si wafer material is however, still under some review with different mechanisms being proposed [20].

It is now generally accepted though that bulk Si must be doped and contain holes before applying an electrochemical etching procedure to initiate pore formation [20]. HF is considered unreactive with a pure bulk Si surface because once it removes any oxide layers it leaves the surface hydrogen terminated with one H atom bound to each surface Si atom. To initiate further reactivity and induce etching, the H-terminated surface must be activated either electrochemically (applying a sufficient voltage) or chemically (adding an oxidant with a sufficient electrode potential). This formation of H bubbles on the surface gives rise to inhomogeneous microporous Si formation [19]. The application of the anodisation cell and potential current results in an electron being removed from the Si-H bond created initially, thus causing a hole (a vacancy in the Si valence band).

The previously passivated Si-H bond is now activated and becomes susceptible to attack by the fluoride solution [21]. Etching now proceeds rapidly inducing pore formation. Once the pore is formed it is the constant potential current that maintains an invariable concentration of HF at the pore tips leading to a more homogenous in-depth porous layer structure being formed [18].

Properties of the Si material such as pore size, volume and depth in this instance, are very much dependant on the anodisation conditions applied, for example: HF concentration, type of wafers (N-type or P-type), crystallographic orientation, current density, anodisation duration [18]. These properties are then tuned to the desired ranges by tailoring the anodisation conditions.

Chemical etching or stain etching applied to Si wafers is a much easier but less frequently employed technique. The key mechanism to form PS is through the etchant solution used (HF, HNO₃ and water (H₂O)). It is believed Nitric Oxide (NO) is produced on the surface of the Si which serves as the hole injector [17]. HNO₃ then serves as the catalyst for porous layer formation [17]. Various mechanisms are again proposed for the overall dissolution chemistry associated with PS formation through this method [17, 22-23] but in general the porous layer structure is formed under similar conditions to the electrochemical etching method discussed previously.

Another key to forming a porous layer structure through chemical etching is the application of certain elements onto the Si surface such as a thin aluminium (Al) film onto a Si substrate [24]. Dimova-Malinovska, D. *et al.* showed that the Al film (up to 200nm in size) actually reacted with the HF

solution and in this case was the mechanism for hole initiation and the porous structure formation [24]. Up to 1 μm thick porous layers on Si wafers can be developed using this method.

Most electrochemical etching procedures can induce porosity up to a few microns thick depending of course on the relative size of the Si wafer or Si particle [17]. Gold (Au) assisted electro-less etching has been seen to cause much deeper pore formation into Si wafers [25]. A nanometre sized Au film ($\sim 4\text{nm}$) is deposited onto doped wafers which upon reaction with the HF based solution causes breaking of the film into tiny Au particles on the surface of the Si wafer.

The applied etching conditions causes pore formation at the position of the Au particles on the surface and relative to the size and morphology of the particles formed [25]. Metal-assisted etching using thin films of platinum (Pt) and silver (Ag) on Si has also been documented as the critical elemental factors to inducing PS formation [26-28].

Incorporating iron (Fe) into HF solutions has also been shown to affect the etching process to some degree [29]. The application of electroless, electrochemical and chemical etching procedures applied to Si is now well documented [22-23].

METALLURGICAL GRADE POROUS SILICON

Metallurgical Grade Porous Silicon (MGPS) powder contains impurities including Fe, Al, Ca, carbon (C) and oxygen (O) [30-32]. During the manufacturing process it is believed that these impurities are a result of the smelting and grinding process applied to make the Metallurgical Grade Silicon (MGSi) powder [30].

Previous studies have shown that MGSi powder contains a host of impurities with Fe, Al and Ca being heavily deposited at the grain boundaries of the material [31]. Vesta Ceramics (Hisings Backa, Sweden) are a leading manufacturing company in producing PS from MGSi powder. They incorporate a jet-milling process on larger particulate sized MGSi powder to break the powder into micron size particles [30].

During the milling process, these powder particles will fracture along grain boundaries where impurities are segregated and therefore particles will have more impurities on the surface. These impurities then react with the chemical etchant applied causing hole initiation and PS formation at the surface relative to the etching rate of Si [30].

METALLURGICAL GRADE POROUS SILICON STRUCTURE

The particle morphology was studied from a series of SEM images, obtained using a Hitachi SU-70 SEM. The images in Figure 1 represent samples 2E-100, 2E-60 and 2E-Bulk. These three samples of MGSi powders are as follows ('2E' refers to the specific grade of material):

- 1) 2E-Bulk – The starting MGSi powder used to make MGPS particles
- 2) 2E-100 – MGPS powder manufactured from the 2E-Bulk powder after chemically etching for 100% of the required etching time (100% etching time is defined as the point when the sample exhibits photoluminescence with an ultraviolet light [30])
- 3) 2E-60 – As for (2) but only chemically etched for 60% of the required etching time.

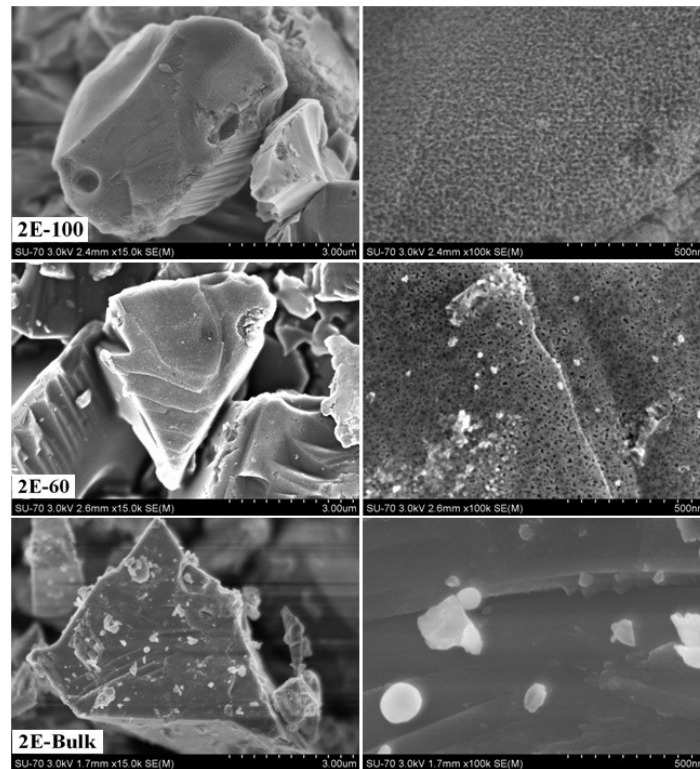


Figure 1. SEM images of selected Si particles in samples 2E-100, 2E-60 and 2E-Bulk.

The MGPS particle size ranges from 4 - 5 μm with pore sizes ranging from 8 - 15 nm in diameter. The random, pitting dispersion of pores on the surface of the MGPS particles is clearly visible. Sample 2E-100 displays a high surface porosity with the surface pores almost coalescing in some cases. The pores in sample 2E-60 are characteristically more spaced out. They also appear shallower in comparison to sample 2E-100. The solid surface of sample 2E-Bulk clearly shows no pore formation prior to the chemical etching process.

Previous studies have used tomography to obtain various morphological characteristics of materials as well as pore information [33-34]. Two MGPS particles were isolated from sample 2E-100 and Transmission Electron Microscopy (TEM) images were recorded at tilt angles about the x-axis ranging from -37° to $+37^\circ$ at 2° intervals.

Using IMOD image analysis software [35], they were then built into a tilt series. From the tilt-series, the core of the MGPS particle in Figure 2a is observed, indicating a thicker core region compared to the outer region of the particle, but it is not possible to tell from the TEM tilt series if this section is porous or not.

In Figure 2b, the tilt series for the smaller MGPS particle, shows that the pores seem to penetrate all the way through.

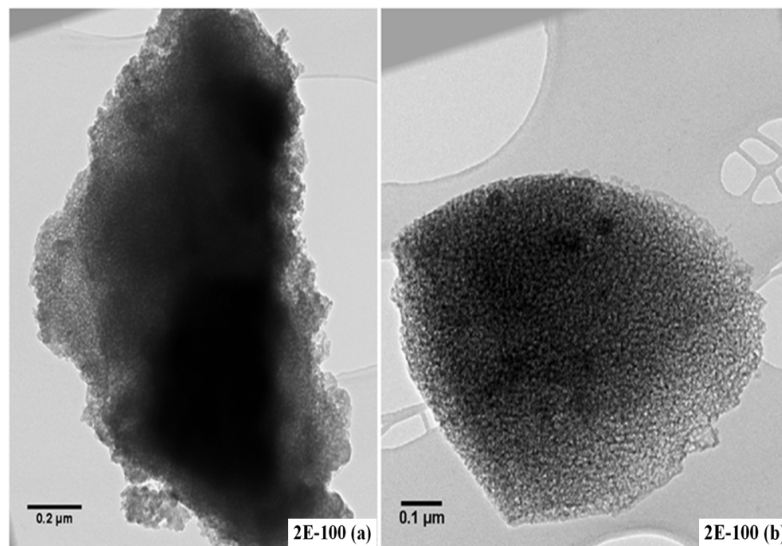


Figure 2. TEM micrographs of MGPS particles (a) and (b) used for tilt series from sample 2E-100.

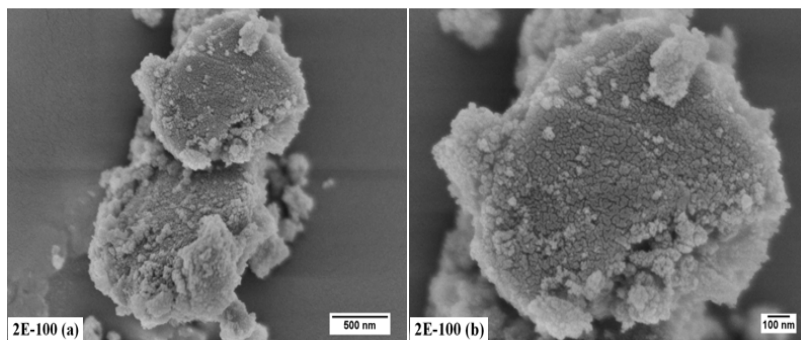


Figure 3. SEM images of fractured particles from sample 2E-100 prepared using a mortar and pestle [32].

The main limitation of this technique in this case is that the particle size is generally too large to allow electrons to penetrate through and is therefore limited to particles with thicknesses of less than approximately 200nm. Due to this limitation, it was not possible to construct a full tomographical series for this sample. A structural study completed by Chadwick et al showed the smaller sized MGPS particles $< 2\mu\text{m}$ in diameter to be completely porous throughout [32]. Larger MGPS particles have a solid Si core and a porous outer shell.

In order to observe the pore structure beneath the surface of the MGPS particles, sample 2E-100 was crushed with a mortar and pestle and analysed with SEM as shown in Figure 3. The results indicate an interconnected pore network existing beneath the surface of the MGPS particles. In keeping with other observations from this study, the pores observed are randomly oriented and numerous. The size of the pore channels range from 7-12nm which also corresponds well to the pore sizes seen in Figure 1 for 2E-100 and 9.6nm for 2E-60 [32].

SIMULATED BODY FLUID

In 1991, Kokubo and Takadama outlined that the essential requirement for an artificial material to bond to living bone *in-vivo* requires the formation of bone-like apatite on its surface and that this *in-vivo* apatite formation could be reproduced using simulated body fluid (SBF) with ion concentrations nearly equal to those of human blood plasma [36]. Thus, the *in-vivo* bone bioactivity can be assessed *in-vitro* using SBF. The formation of a bone-like apatite layer

on the surface of a material creates the bond between the substrate material and living bone. Bioactive glasses, apatite containing glass-ceramics, composite glass-ceramics, sintered HA and apatite β -tricalcium phosphate biphasic ceramic were all found to produce an apatite layer on their surface in SBF and when implanted *in-vivo* they also bonded to living bone through formation of a CaP apatite layer [36]. Thus, the direct correlation between *in-vitro* results and *in-vivo* results are once again clarified.

The precipitation of bioactive calcium phosphate in SBF is governed by complex thermodynamics, consisting of seventeen association / disassociation reactions [37]. SBF is a supersaturated solution with respect to apatite; however, it does not spontaneously deposit apatite during storage at 36.5°C indicating that the degree of supersaturation is not so high as to induce homogeneous apatite nucleation. Tanihara *et al.* identified the factors, which govern heterogeneous apatite nucleation on a substrate [38]. The rate, I , of heterogeneous nucleation of a crystal on a substrate in a solution at temperature T is given by Equation 1:

$$I = I_o \exp\left(\frac{\Delta G}{kT}\right) \exp\left(\frac{\Delta G_m}{kT}\right) \quad (\text{Equation 1})$$

where:

ΔG is the free energy for the formation of an embryo of crystal size

ΔG_m is the activation energy for transport across the nucleus-solution interface.

Of these ΔG_m is independent of the substrate. ΔG is given by Equation 2.

$$\Delta G = 16O^3 f(\theta) / 3(kT/V_\beta \ln(IP/K_0)) \quad (\text{Equation 2})$$

where:

σ = the interface energy between the nucleus and the solution.

IP = the ionic activity product of the crystal in the solution.

K_0 = the value of IP at equilibrium (the solubility of the crystal).

$f(\theta)$ = a function of constant angle between the nucleus and the substrate.

V_β = the molecular volume of the crystal phase.

Among these terms $f(\theta)$ depends on the substrate and IP/K_0 , a measure of the degree of supersaturation also depends on the substrate when the

substrate releases some constituent ions of the crystal. Therefore an increase in the ionic activity product or a decrease in $f(\theta)$ is effective for heterogeneous apatite nucleation [37]. An increase in the ionic activity product of apatite can be facilitated by release of Ca^{2+} , PO_4^{3-} , or OH^- , which are constituents of apatite. Among these, Tanihara *et al.* state that increasing Ca^{2+} is most effective [38].

Lu and Leng carried out thermodynamic and kinetic analysis of SBF and found that HA precipitation exhibits a higher thermodynamic driving force than octacalcium phosphate (OCP) or dicalcium phosphate dehydrate (DCPD) even though OCP precipitation is kinetically favourable in SBF. Similarly, DCPD does not have a thermodynamic driving force of precipitation in SBF, even though it has kinetic advantages in nucleation. Generally, precipitation of carbonate-containing HA is more kinetically favourable than that of stoichiometric HA and has the same level of thermodynamic driving force; precipitation of calcium-deficient HA is also more kinetically favourable, but its thermodynamic driving force is lower than that of stoichiometric HA [37].

On the basis of the thermodynamic principals that govern apatite precipitation, a mechanism of apatite formation can be explained. There are two important factors pertaining to apatite formation in SBF. The first is the release of ionic species to increase the degree of supersaturation of the surrounding fluid with respect to apatite, the other is the existence of favourable sites for heterogeneous nucleation. For bioglass, the following mechanism is proposed. Upon immersion in SBF, dissolution of the material's surface occurs and results in the release of Ca^{2+} ions into solution and the formation of Si-OH groups. At the interface, the degree of supersaturation of SBF increases with respect to apatite until the free energy barrier for the formation of a critical nucleus ΔG is reached. Once reached, crystal nucleation begins at precise sites along the substrate surface and crystals attach at specific sites along the substrate (*e.g.* Si-OH groups). Once the critical nucleus is attached to the substrate it grows by the ionic deposition of Ca^{2+} , PO_4^{3-} and OH^- from solution onto the growing nucleus, with neighbouring crystals imposing space restrictions thus governing the direction of the growth. The process continues until the surface has been fully covered and a bioactive surface layer of CaP has been formed. It has been speculated that apatite formation on silica gel is induced by silanol groups on its surface. However, it has also been proposed that pores play an important role in nucleating the apatite, rather than the silanol groups [39-40]. In studies by Pereira *et al.* induction time for apatite formation on a silica gel in SBF was shown to

increase with decreasing pore volume and pore size, as such it was postulated that negatively charged pores larger than a 2 nm radius provide favourable conditions for the apatite nucleation and hence act as nucleation sites [41-42]. On the other hand, West and Hench proposed, on the basis of molecular orbital calculations, that surface defects such as trisiloxane rings are effective for the apatite nucleation [43].

Cho *et al.* found that neither the presence of the silanol groups nor that of the trisiloxane rings is a sufficient condition for apatite nucleation and that the presence of pores larger than 1.7 nm is also an insufficient condition for the apatite nucleation [44]. However, it was speculated that a certain type of structural unit of silanol groups was effective for apatite nucleation.

It is important to note at this point that while SBF *in vitro* tests are considered an essential 'guide' for predicting *in-vivo* bioactivity and determining the bone bonding ability of a material, it is also possible for some materials to invoke a successful *in-vivo* response even though they were unsuccessfully trialed in SBF. Böhner and Lemaître outlined certain aspects of the current and established SBF which is used by many researchers, which could be improved upon to further resemble blood serum [45]. It is proposed that the simplest SBF solution should be in equilibrium with DCPD [45]. The current SBF used however, is also established as the main method for exploring potential *in-vitro* bioactivity.

POROUS SILICON BIOMATERIALS AND BIOACTIVE SILICON COATINGS

Biomaterials are a select group of materials used for medical treatment within the human body [46]. They can be either modified natural or synthetic materials which find application in a wide variety of medical and dental implants and prosthesis used for repairing, enhancing or replacing natural tissues [47]. A key element of biomaterials is that they must assist in a medical function or capacity while maintaining compatibility with human organs and tissues [46]. Examples of clinical biomaterial applications today include joint replacement, vascular grafts and heart valves [47]. In terms of potential bio applications of Si and PS materials, research is currently underway exploring the use of Si and PS for enhancing current medical device coatings by producing composite materials and also exploring the use of Si and PS as a standalone coating material, as well as drug delivery devices.

A novel approach to creating potential bioactive mesoporous silica coatings for implants was outlined by Gomez-Vega *et al.* in 2001. Here, Si substrates were etched in HF (5 vol. %) for 30 seconds to remove a silica layer. A substrate of Ti6Al4V was then coated with the mesoporous silica film (0.1 to 1µm) through a spin casting method using sol-gels as described [48]. After immersion for 7 days in SBF, hemispherical formations of apatite crystals with a leaf-like texture were observed on the surface of the coating material [48]. This outcome *in-vitro*, is indicative of the potential bone bonding ability of this bioactive coating material *in-vivo* [49].

Since HA is already known to be bioactive and osteoconductive, it is therefore the current bioactive coating of choice for metallic implants. Investigations into combining this already osteoconductive material with Si and PS are underway due to the potential to enhance the bioactive properties, bonding ability and life-span of the coating at the implant-bone interface [50-52]. Si itself is thought to positively affect the cellular response at the implant-bone interface since Si is present in high concentration in metabolically active osteoblasts and considered critical in extracellular matrix formation in bone and cartilage [50]. Thian *et al.* investigated the *in-vitro* bioactivity of Si-doped HA coatings applied to a titanium substrate through magnetron co-sputtering in SBF. When comparing the as-sputtered HA (control sample) and Si-doped HA coatings it was revealed that a denser precipitated layer formed on Si-doped HA showing improved bioactivity compared to the as-sputtered HA material [50]. The increased bioactivity of the Si-doped HA can be attributed to the chemical reactions between the SBF and the coating material. During the initial dissolution phase Ca (Ca^{2+}) and P (P^{5+}) ions are released into the SBF which increases the degree of super-saturation of SBF with respect to apatite. This facilitates the initial formation of CaP nuclei on the coating surface by consuming the Ca^{2+} and P^{5+} in the SBF [50]. CaP crystallite growth results in combination with the formation of additional nuclei creating a surface apatite layer.

It is suggested that the incorporation of Si into the HA coatings results in Si^{4+} ions also attaching to the surface of the coating as SiO_4^{4-} ions thus inducing further sites for nucleation and crystallization of the apatite layer [50]. Annealing the sample has also been shown to increase the rate at which the apatite layer forms *in-vitro*. Gibson *et al.* has also reported that the incorporation of Si into HA enhances osteoblast cell activity and increases apatite formation in SBF when compared to phase-pure HA [53]. Sanchez *et al.* explored the modification of a PS substrate by coating with HA through cathodic bias in an electrochemical process in a cell culture study [54]. The

resultant material proved to have positive results showing proliferation of macrophages on the surface of the modified PS-HA material [54].

An improvement in the mechanical properties of Si-incorporated coralline HA to Porous HA was achieved by Kim *et al.* showing an increase in compressive strength of up to 5.5 Mpa [55]. Niu *et al.* explored vacuum plasma spraying of Si coatings onto Ti6Al4V and showed improved *in-vitro* bioactivity when the samples were cleaned prior to SBF treatment at high temperature using de-ionized water [56]. It is proposed that the Si-OH groups which exist on the surface of the Si coating react with the hydroxyl ions in the SBF creating a negative charged surface with a Si-O⁻ functional group [56]. This negative surface then attracts positive Ca²⁺ ions which are the first crucial ions needed to form an apatite layer. Adsorption of the Ca ions onto the surface coating results in hydrated precursor clusters containing Ca Hydrogen P. These clusters then grow by consuming the CaP ions in the SBF forming an amorphous CaP phase which later crystallizes into carbonate containing HA [56].

The structure of the bond between bone and PS substituted HA was explored by Porter *et al.* in 2005 [57]. This *in-vivo* study explored the PS-HA bioceramic after it was placed into the distal femur of a rabbit and examined after a 6 week period. Results showed the growth of organized collagen fibers into the strut porosity at the bone PS-HA implant interface which then formed into mineralized fibrils within the implant [57]. It was observed that the apatite crystallites directly abutted and overlaid the Si-HA grains. Hence bone simply weaves over Si-HA forming a mechanical interlock and biological bond to the underlying ceramic [57].

The majority of Si-HA coatings can be applied using plasma spraying, magnetron co-sputtering, sol-gel and pulse laser deposition [58]. Li *et al.* reported on the formation of uniform Si-HA phase coatings up to 1.4µm thick on commercially pure Ti substrates using an electrochemical deposition technique in electrolytes containing Ca²⁺, PO₄³⁻ SiO₃³⁻ ions with various molar ratios (n_{si}) [58]. This particular technique had a negative drawback which showed that the presence of Si in the electrolyte acts as an inhibitor to the growth of Si-Ha crystals leading to a decrease in potential coating thickness and results in overall changes to the HA crystal structure due to the loss of some OH ions [58]. Zhang *et al.* studied the effects of HA and Si-HA coatings applied to porous Ti [59]. The porous Ti which had a pore size of up to 150-600µm and a porosity of 67%, was prepared using a fiber sintering process.

The HA and Si-HA coatings were applied to the porous Ti through a biomimetic coating process. *In-vivo* studies showed that the Bone In-Growth

rate (BIR) of the HA and Si-HA coatings were significantly higher than the uncoated porous Ti and that overall the Si-HA coated porous Ti displayed significantly higher BIR and highly improved surface bioactivity than the HA coated porous Ti [59]. Another study was conducted by Zhang *et al.* exploring the bioactivity of Si incorporated TiO_2 (Si- TiO_2) coatings compared to TiO_2 coatings and Ti plates [60]. The Si- TiO_2 coating was prepared by Micro-Arc Oxidation (MAO) in a Ca, P, Si containing electrolyte. MAO is a plasma assisted electrochemical method that produces thick, rough and nano-structured oxide films on Ti. Here MC3T3-C1 osteoblastic cells were seeded onto the three substrates with the Si- TiO_2 showing the greatest cell attachment and proliferation. This was attributed to the Si releasing from the TiO_2 contributing to extracellular pH changes causing the structural alteration of the cell transmembrane proteins [60]. These altered proteins interact and bond with proteins adsorbed on the Si- TiO_2 coatings from the culture medium promoting the attachment of the cells onto the surface. The porous surface structure is also thought to play a key role in attachment and proliferation [60].

POROUS SILICON IN DRUG DELIVERY AND THERAPEUTICS

PS is increasingly being investigated for use as a potential material for drug delivery and therapeutics given its unique properties including high drug loading capacity, tunable surface porosity, heat and radiation stability, *in-vivo* biocompatibility and controlled release properties [61]. Prestidge *et al.* studied the loading of a model hydrophilic protein - papain into stain etched and anodized PS powders. Analysis concluded that the papain burst and sustained release is dependent on the PS type and loading level and that the loading of the protein was more efficient for the anodized PS than the stain etched PS [61]. Mesoporous Si microparticles were produced using thermal carbonisation (TCPSi) and thermal oxidation (TOPSi) to create particle surfaces which were suitable for drug administration applications [62]. The loading of five drugs (antipyrine, ibuprofen, griseofulvin, ranitidine and furosemide) into the microparticles and their subsequent release behavior was examined [62]. The loading efficiencies varied between 9%-45% while the release rate was dependant on the characteristic dissolution behavior of the drug substance. When the dissolution rate was high the microparticles caused a delayed release [62]. Providing controlled and localised release of therapeutics

within the body are essential objectives for improving efficiency and reducing the risks of potential side effects [1].

The low toxicity of PS, its high porosity and tunable surface chemistry has created a surge of interest in developing PS as a potential mothership for therapeutics, diagnostics and other types of payloads [1]. PS was previously explored as a potential therapeutic agent for cancer treatment [63]. Photodynamic therapy (PDT) has some short and long-term side effects arising from reactive oxygen species (ROS). Single-walled carbon nano tubes (CNT) combined with near-infrared (NIR) light irradiation developed significant interest due to their heat generation capability and potential to develop them as therapeutic nano-bomb agents [63]. This particular PS study showed that the surface temperature of PS increased as quickly and as high as CNT and this generated heat is sufficient to kill off cancer cells. The PS was also found to produce smaller amounts of ROS than CNT during NIR light irradiation [63].

Mesoporous Si was developed as a multistage delivery system for imaging and therapeutic applications [64]. The mesoporous Si particles were biodegradable and biocompatible with well controlled shapes, sizes and porosity and able to carry, release over time and deliver nanoparticles to primary endothelial cells [64]. Another study investigated the interaction of B50 rat hippocampal cells with stain-etched PS [65]. These cells showed a clear preference for the PS material surface compared to an untreated surface and it was observed that the network pattern is influenced by a single neuron response to the material surface nature and topology [65]. Mesoporous silica nanoparticles (MSN's) showed the ability to carry basic fibroblast growth factors (bFGF), proteins which play a key role in wound healing and blood vessel regeneration [66]. PS is similar to MSN's in that they have well documented surface properties, tunable pore sizes and very large surface areas making them ideal candidates for drug delivery devices, therapeutics and cell culture mediums and general biocompatible materials for a wide range of applications.

ANALYSIS OF A BIOACTIVE METALLURGICAL GRADE NANO-POROUS SILICON PTFE COMPOSITE

A polytetrafluoroethylene (PTFE) MGPS composite sheath structure was purchased from Vesta Sciences (Hisings Backa, Sweden). This composite consisted of fused PTFE beads (Dupont No.60 Teflon™) with embedded

MGSi microparticles which had been chemically etched to produce a nanoporous structure.

The MGSi microparticles were chemically etched in a similar fashion to sample 2E-100 (2E-100 – MGPS powder manufactured from the 2E-Bulk powder after chemically etching for 100% of the required etching time (100% etching time is defined as the point when the sample exhibits photoluminescence with an ultraviolet light [30])). Particle size was around 4 μ m with the surface area at 157m²/g, pore volume at 0.3cc/g and pore size is an average of 5.9nm. SBF was produced in accordance with published methods [36, 67].

Reagents were dissolved in sequential order (as per Table 2) into 500 mL of purified water (Reagecon, Shannon, Ireland) using a magnetic stirrer. The solution was maintained at 36.5 \pm 1.5 $^{\circ}$ C using a water bath. One mole HCl was titrated to adjust the pH of the SBF to 7.40. Purified water was then added to adjust the total volume of liquid to one litre. Once prepared, the SBF was stored for 24 h (5 $^{\circ}$ C) to ensure that no precipitation occurred.

Composite structures were cut into appropriately sized samples and immersed in a calculated quantity of simulated body fluid (SBF), such that equation 3 was satisfied:

$$V_s = S_a/10 \quad \text{(Equation 3)}$$

where V_s is the volume of SBF (ml) and S_a is the surface area of the specimen (mm²). Specimens in SBF were stored in plastic containers and maintained at 37 \pm 1 $^{\circ}$ C for 1, 7 and 14 days. After removal from SBF, each sample was gently rinsed with purified water, placed on individually labelled sheets of filter paper and left in desiccators at room temperature to dry. After removal from SBF solutions, a JEOL JSM-840 scanning electron microscope (JEOL Ltd., Tokyo, Japan) equipped with a Princeton Gamma Tech (PGT) Energy Dispersive X-ray (EDX) system (Princeton Gamma Tech UK Ltd., Peterborough, UK) was used to obtain secondary electron images and carry out chemical analysis of the surface of the composites. All EDX spectra were collected at 20 kV, using a beam current of 0.26 nA. Quantitative EDX converted the collected spectra into concentration data by using standard reference spectra obtained from pure elements under similar operating parameters. A Phillips Xpert MPD Pro 3040/60 X-ray Diffraction (XRD) Unit (Phillips, Amsterdam, Netherlands) was used to perform thin film XRD (TF-XRD) on the surface of the composites after immersion in SBF to analyze the crystallinity of the CaP layer formed.

Table 2. Order and amounts of reagents used to prepare 1,000 mL of SBF

Order	Reagent	Quantity
1	NaCl	8.035 g
2	NaHCO ₃	0.355 g
3	KCl	0.225 g
4	K ₂ HPO ₄ ·3H ₂ O	0.231 g
5	MgCl ₂ ·6H ₂ O	0.311 g
6	1.0 M-HCl	39 mL
7	CaCl ₂	0.292 g
8	Na ₂ SO ₄	0.072 g
9	Tris	6.118 g
10	1.0 M-HCl	0–5 mL

TF-XRD was run between 25 and 45 degrees 2-theta, using a generator voltage of 40 Volts and a tube current of 40 Amps, a step size of 0.017 degrees 2-theta and a step time of 40.72 s. A Varian 610-IR Attenuated Total Reflection Fourier Transform Infrared (ATR-FTIR) spectrometer was used to examine changes to the functional groups of the samples after each time period of immersion in SBF. 32 ATR-FTIR scans were averaged between 4000 and 500 cm⁻¹, with a resolution of 4 cm⁻¹. The SBF solutions, after removal of the composite material, were filtered using Watman filter paper (1µm nominal pore size) and acidified (to maintain dissolution and prevent any re-precipitation during analysis) by making up 5 ml of SBF to 25 ml using 2 vol.% nitric acid. Standards were purchased (Reagecon, Shannon, Ireland) and suitably diluted, such that a linear correlation could be made within the range of the SBF samples. Inductively Coupled Plasma-Optical Emission Spectroscopy (ICP-OES) was run on standards and samples and 2 vol. % nitric acid was used to clean out lines between runs.

As indicated in Figure 4, the MGPS particles are clearly visible above the teflon tape. As might be expected, SEM-EDS analysis reveals only the presence of Si, O and fluorine (F), (Figure 5a) which are due to Si from the particles, F from the etching process and O from the surface oxide on the teflon tape [32]. However, post-immersion in SBF, the MGPS-PTFE composite exhibits precipitation of a needle-like morphology on its surface. EDX analysis reveals that this precipitate consists of Ca, P and Si, with small amounts of sodium (Na) and magnesium (Mg) incorporation (Figure 5b). From the SEM analysis it was evident that the MGPS-PTFE composite could induce the rapid formation of bone-like apatite on its surface in SBF.

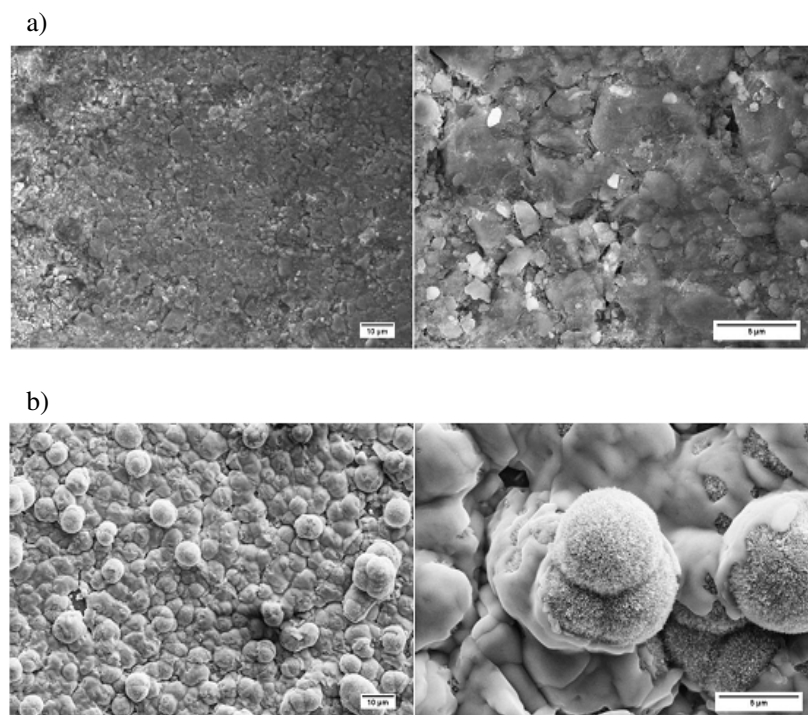
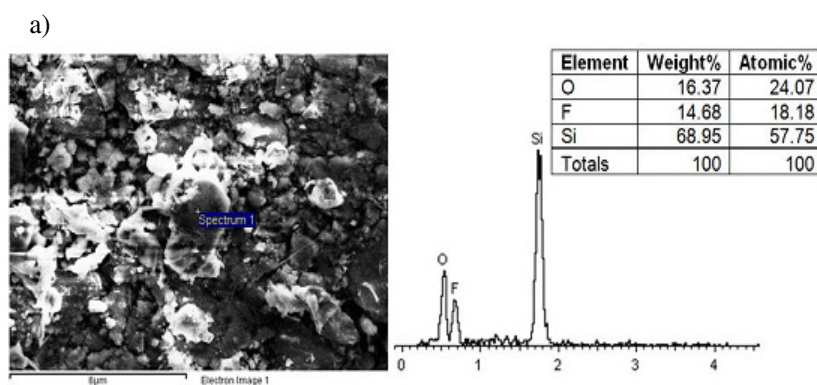


Figure 4. SEM of the MGPS-PTFE composite before (a) and after (b) immersion in SBF for 14 days.

Apatite spherulites formed on the MGPS-PTFE of $> 1\mu\text{m}$ in size were observed after 14 days in SBF and the Ca/P ratios observed were consistent with HA of 1.67 [67].



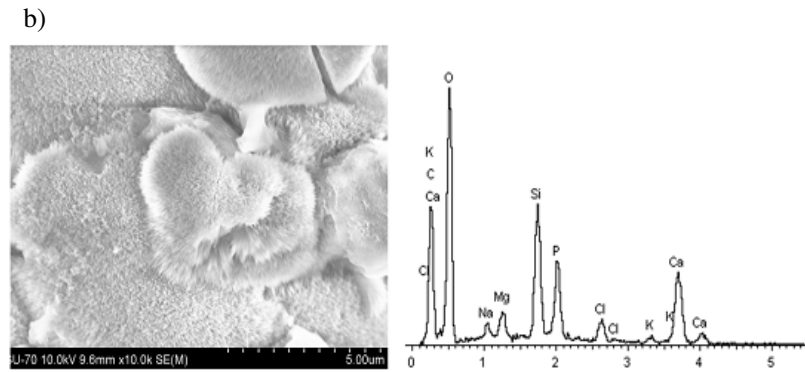


Figure 5. EDX analysis of MGPS-PTFE composite before (a) and after (b) immersion in SBF.

Thin film X-ray diffraction (TF-XRD) of the fully etched sample (Figure 6) reveals that the precipitate is crystalline in nature and is indeed crystalline HA.

It can be observed from Figure 6 that after only 1 day of immersion in SBF there is evidence of a small HA peak at approximately 26 degrees 2-theta. This 100% HA peak continues to grow between 1 and 14 days of immersion in SBF, relative to the background Si peak, present at approximately 28.5 degrees 2-theta.

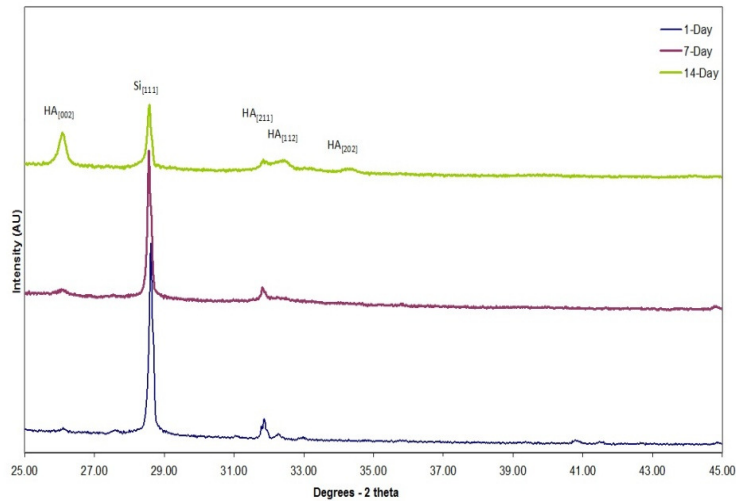


Figure 6. TF-XRD of the MGPS-PTFE composite at different immersion times in SBF.

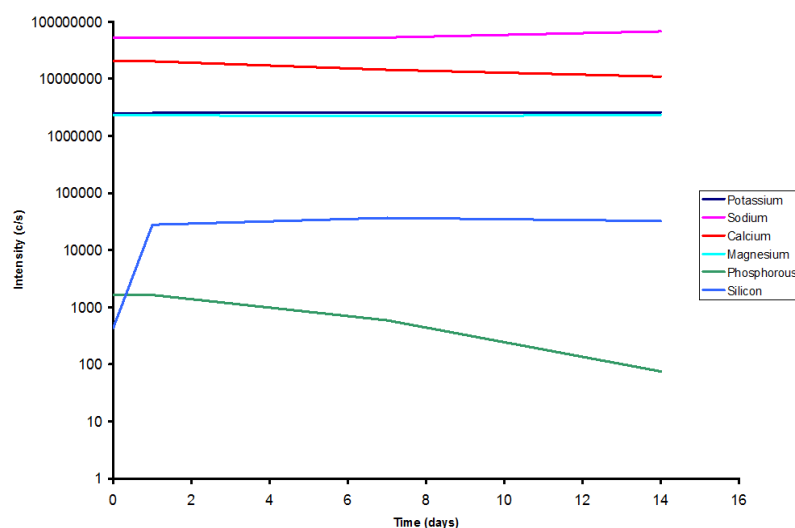


Figure 7. ICP-OES of SBF after different periods of MGPS-PTFE composite immersion.

Inductively coupled plasma-optical emission spectroscopy (ICP-OES) analysis of the remaining SBF solutions after immersion studies indicated a linear reduction in Ca and P content with immersion time (Figure 7), as might be expected with the surface precipitation of HA on the composite. However, Si content in the solution was observed to increase after 1 day of immersion and linearly decrease thereafter. This would indicate that initial degradation of the Si particles occurs, followed by uptake by the precipitating HA. This indicates that the initial HA precipitation observed (after 1 day) may be either Si free or have a low Si content, followed thereafter (7 and 14 days) by precipitation of a Si-rich HA phase. This initial Si release into solution, as well as the subsequent uptake in the HA structure will likely be beneficial from a therapeutic prospective.

The microparticles used in this MGPS-PTFE composite material are similar to the ones used in a previous study by Chadwick, Clarkin and Tanner which showed that the powder induced bone-like apatite formation on its surface in SBF [67]. Previous TEM analysis of the surface of the MGPS particles indicated the presence of a dense surface layer of large particle-like aggregates of needle shaped crystals, typified by the image in Figure 8a. Nano-beam diffraction analysis indicated a crystalline structure as shown by Figure

8b. The crystal structure was matched to HA in the JPDS database (reference number 01-1008) [67].

The simulated diffraction pattern is indicated in Figure 8b. The results shown were found to be representative of the sample as a whole, after a number of different areas were studied. The compositional elements of the surface layer, as identified by EDX indicate the presence of Ca, P and Si within the crystalline structure (see Figure 8c). The lower region on the left of the image in Figure 8a shows the MGPS area covered by the dense crystalline apatite layer.

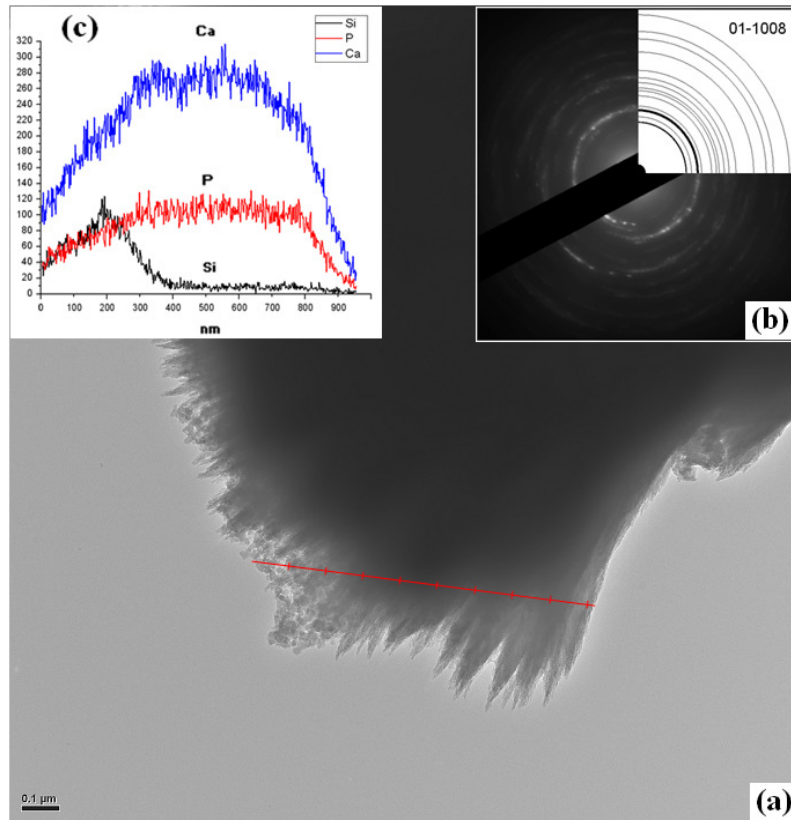


Figure 8. (a) Bright Field TEM micrograph of surface apatite layer of sample (a) after 30 day immersion in SBF (b) Nano-Beam diffraction pattern from (a) showing crystalline structure (c) Inset on the top left shows the Line-EDX analysis starting from left to right as indicated by the line at the bottom of the image (The MGPS region is on the left of the line while the needle-like apatite structure is on right) [67].

The line across this selected area represents the TEM Line EDX spectra in Figure 8c. The high Si peak shows the initial MGPS region which is then covered by the apatite layer and represented by high Ca and P peaks [67].

CONCLUSIONS

PS has the potential to serve as a biomaterial with a wide range of applications. It has both tunable and controllable surface properties and characteristics favouring the material ahead of most other potential applications. It has already been proven as biocompatible, biodegradable and can also assist in tailoring current market biomaterials and surface coatings to have improved bioactivity both *in-vitro* and *in-vivo*. PS is increasingly being investigated for drug delivery and therapeutic applications given its unique properties including high drug loading capacity, surface porosity, heat and radiation stability, and controlled release properties. Current orthopedic devices consist mainly of CoCr or Ti which are then surface coated with HA to induce osteointegration and bone bonding *in-vivo*. PS and Si has been shown to enhance this bone bonding ability and improve the bioactivity of such devices by incorporation of Si into HA. Given the drug loading capabilities of PS one could develop a suitable device which not only improves the bioactivity of current market HA coatings but which could be fully loaded with growth factors to further stimulate bone healing at the implant site. This would result in a longer lasting and a more permanent solution to current orthopaedic implants and would also allow greater health benefits for the patient. The potential to expand and combine this research and further integrate it into the therapeutics fields seems limitless. The authors also present current work on characterising bioactive MGPS particles and a bioactive MGPS-PTFE composite material which have the potential to be further developed for suitable bone bonding applications or a guided bone regeneration device. The composite material was examined after SBF trials and initiated deposition of a 'bone-like apatite' on its surface after only 1 day of immersion. This 'bone-like apatite' contains Si incorporated into its structure, which is known to improve apatite's biocompatibility and results in increased cellular differentiation and bone growth. Due to its reactivity *in-vitro* and its nanoporous sponge structure, this material exhibits potential for use in bony applications, as well as in drug delivery device applications. This device may be used as an enhanced bioactive platform for the incorporation and delivery of various pharmacological and biological agents *in-vivo*.

ACKNOWLEDGEMENTS

The Authors would like to acknowledge the financial support of Enterprise Ireland, Vesta Sciences (EI IP 2007 0380 Vesta/ UL), PRTL cycle 4 and Waterford Institute of Technology's South Eastern Applied Research Centre. They would also like to thank Vesta Sciences and Dr Shanti Subramanian for providing MGPS samples. The authors thank Vishnu Mogli, Paula Olsthoorn, Gaye Hanrahan, Dr. Calum Dickinson, Dr. Gordon Armstrong, Dr. Tofail Syed, Dr. Wynette Redington Dr. Fathima Laffir, Dr. Colm O' Dwyer, Dr. Serguei Beloshapkin, Dr. Ramesh Raghavendra and Professor Shohei Nakahara for analytical results and useful discussion.

REFERENCES

- [1] Anglin, E.J., et al., Porous silicon in drug delivery devices and materials. *Advanced Drug Delivery Reviews*, 2008. 60(11): p. 1266-1277.
- [2] Jugdaohsingh, R., et al., Dietary silicon intake is positively associated with bone mineral density in men and premenopausal women of the Framingham Offspring cohort. *Journal of bone and mineral research : the official Journal of the American Society for Bone and Mineral Research*, 2004. 19(2): p. 297-307.
- [3] Carlisle, E.M., Silicon: a possible factor in bone calcification. *Science* (New York, N.Y.), 1970. 167(3916): p. 279-280.
- [4] Carlisle, E.M., Proceedings: Silicon as an essential element. *Federation proceedings*, 1974. 33(6): p. 1758-1766.
- [5] Henstock, J.R., *Porous Silicon - Polycaprolactone Composites for Orthopaedic Tissue Engineering*, in School of Biomedical Sciences, Medical School, University of Nottingham, UK. 2009.
- [6] Porter, A.E., Nanoscale characterization of the interface between bone and hydroxyapatite implants and the effect of silicon on bone apposition. *Micron* (Oxford, England : 1993), 2006. 37(8): p. 681-688.
- [7] Gibson, I.R., S.M. Best, and W. Bonfield, Chemical characterization of silicon-substituted hydroxyapatite. *Journal of biomedical materials research*, 1999. 44(4): p. 422-428.
- [8] Patel, N.B., S.M. Bonfield, W. Gibson, I.R. Hing, K.A. Damien, E. Revell, P.A., A comparative study on the in vivo behaviour of

- hydroxyapatite and Silicon substituted hydroxyapatite granules. *Journal of Materials Science: Materials in Medicine*, 2002. 13: p. 1199-1206.
- [9] Ishizaki, K., S. Komarneni, and M. Nanko, *Porous Materials: Process technology and applications*. 1998: Kluwer Academic Publishers.
 - [10] Ratner, B.D., et al., *Biomaterials Science: An Introduction to materials in medicine*. Vol. Second edition. 2004: Elsevier Academic Press: Copyright 2004.
 - [11] Gorbanyuk, T.I., et al., Porous silicon microstructure and composition characterization depending on the formation conditions. *Thin solid films*, 2006. 495(1-2): p. 134-138.
 - [12] Fuchs, A. Adsorption and Separation Processes in Nano-Porous Materials. in *Pacific Rim Conference in Nanoscience*. 2004.
 - [13] du Plessis, M. *Integrated Nanoporous Silicon Nano-explosive Devices*. 2007.
 - [14] Foss, S.E., *Graded Optical Filters in Porous Silicon for use in MOEMS Applications*, in Department of Physics, Faculty of Mathematics and Natural Sciences. 2005, University of Oslo.
 - [15] Pap, A.E., *PhD-Investigation of pristine and oxidised porous silicon*, in Faculty of Technology, Department of Electrical and Information Engineering. 2005, University of Oulu: Infotech Oulu.
 - [16] Parkhutik, V., Analysis of publications on porous silicon: from photoluminescence to biology. *Journal of Porous Materials*, 2000. 7(1): p. 363-366.
 - [17] Coffey, J.L., Porous Silicon Formation by Stain Etching, in *Properties of Porous Silicon*, L. Canham, Editor. 1997, INSPEC-The Institution of Electrical Engineers. p. 23-29.
 - [18] Halimaoui, A., Porous Silicon Formation by Anodisation, in *Properties of Porous Silicon*, L. Canham, Editor. 1997, INSPEC-The Institution of Electrical Engineers. p. 12-22.
 - [19] Gosele, U. and V. Lehmann, Porous silicon quantum sponge structures: Formation mechanism, preparation methods and some properties, in *Porous Silicon*, Z.C. Feng and R. Tsu, Editors. 1995, World Scientific Publishing Co: New York. p. 17-39.
 - [20] Bisi, O., S. Ossicini, and L. Pavesi, Porous silicon: a quantum sponge structure for silicon based optoelectronics. *Surface Science Reports*, 2000. 38(1-3): p. 1-126.
 - [21] Arrand, H., *Optical Waveguides and Components Based on Porous Silicon*. 1997, University of Nottingham: Nottingham. p. 102.

-
- [22] Kolasinski, K., Silicon nanostructures from electroless electrochemical etching. *Current Opinion in Solid State and Materials Science*, 2005. 9: p. 11.
 - [23] Zhang, X.G., Morphology and Formation Mechanisms of Porous Silicon. *Journal of the Electrochemical Society*, 2004(151): p. 69-80.
 - [24] Dimova-Malinovska, D., et al., Preparation of thin porous silicon layers by stain etching. *Thin Solid Films*, 1997. 297(1-2): p. 9-12.
 - [25] Megouda, N., et al., Au-assisted electroless etching of silicon in aqueous HF/H₂O₂ solution. *Applied Surface Science*, 2009. 255(12): p. 6210-6216.
 - [26] Chattopadhyay, S., X. Li, and P.W. Bohn, In-plane control of morphology and tunable photoluminescence in porous silicon produced by metal-assisted electroless chemical etching. *Journal of Applied Physics*, 2002. 91(9): p. 6134-6140.
 - [27] Douani, R., et al., Formation of aligned silicon-nanowire on silicon in aqueous HF/(AgNO₃ + Na₂S₂O₈) solution. *Applied Surface Science*, 2008. 254(22): p. 7219-7222.
 - [28] Yae, S., et al., Formation of porous silicon by metal particle enhanced chemical etching in HF solution and its application for efficient solar cells. *Electrochemistry Communications*, 2003. 5(8): p. 632-636.
 - [29] Solomon, I., et al., Intense photoluminescence of thin films of porous hydrogenated microcrystalline silicon. *Journal of Applied Physics*, 2008. 103(8): p. 083108-083108-4.
 - [30] Subramanian, S., S.Y. Limaye, and D. Farrell, *Silicon Nanosponge Particles*. 2006: Ireland.
 - [31] Kareh, K., A. Ghahremaninezhad, and E. Asselin, Electrochemical properties of metallurgical-grade silicon in hydrochloric acid. *Electrochimica Acta*, 2009. 54(26): p. 6548-6553.
 - [32] Chadwick, E., S. Beloshapkin, and D.A. Tanner, Microstructural Characterisation of Metallurgical Grade Porous Silicon Nanosponge Particles. *Journal of Materials Science*, 2011.
 - [33] Messaoudi, C., et al., TomoJ: tomography software for three-dimensional reconstruction in transmission electron microscopy. *BMC Bioinformatics*, 2007. 8(1): p. 288.
 - [34] Kim, M.J., et al., Characteristics of solid-state nanometre pores fabricated using a transmission electron microscope. *Nanotechnology*, 2007. 18: p. 5.

-
- [35] Kremer, J., D. Mastrorade, and J. McIntost, Computer visualisation of three-dimensional image data using IMOD. *Journal of Structural Biology*, 1996. 116: p. 71-76.
 - [36] Kokubo, T. and H. Takadama, How useful is SBF in predicting in vivo bone bioactivity? *Biomaterials*, 2006. 27(15): p. 2907-2915.
 - [37] Lu, X. and Y. Leng, Theoretical analysis of calcium phosphate precipitation in simulated body fluid. *Biomaterials*, 2005. 26(10): p. 1097-1108.
 - [38] Tanihara, M., Miyazaki, T., Ogata, S-I., Ohtsuki, C., , Design and Development of Functional Biocompatible Hybrid Materials for Medical Applications, in *Handbook of Organic-Inorganic Hybrid Materials and Nanocomposites*. 2003, American Scientific Publishers. p. 265-293.
 - [39] Cho, S.-B., et al., Dependence of Apatite Formation on Silica Gel on Its Structure: Effect of Heat Treatment. *Journal of the American Ceramic Society*, 1995. 78(7): p. 1769-1774.
 - [40] Kokubo, T., Dependence of Bone-like Apatite Formation on Structure of Silica Gel, in *Bioceramics 7*, O.H. Eds Anderson, Urpo, A. Y., Editor. 1994, Butterworth-Heinemann, Oxford. p. 49.
 - [41] Pereira, M.M., A.E. Clark, and L.L. Hench, Effect of Texture on the Rate of Hydroxyapatite Formation on Gel-Silica Surface. *Journal of the American Ceramic Society*, 1995. 78(9): p. 2463-2468.
 - [42] Pereira, M.M. and L.L. Hench, Mechanisms of hydroxyapatite formation on porous gel-silica substrates. *Journal of Sol-Gel Science and Technology*, 1996. 7(1-2): p. 59-68.
 - [43] J. H. WEST and L. L. Hench, , edited by Bioceramics, ed. T.K.a.T.N.K.K. T. Yamamuro, Kyoto). Vol. Vol. 5. 1991.
 - [44] Cho, S.B., et al., Apatite formation on silica gel in simulated body fluid: effects of structural modification with solvent-exchange. *Journal of materials science. Materials in medicine*, 1998. 9(5): p. 279-284.
 - [45] Bohner, M. and J. Lemaitre, Can bioactivity be tested in vitro with SBF solution? *Biomaterials*, 2009. 30(12): p. 2175-2179.
 - [46] Heleno Rocha Alves, N.S.W., Jose R.T. Branco, Performance Evaluation of Hydroxyapatite Coatings Thermally Sprayed on Surgical Fixation Pins. *Key Engineering Materials (Volumes 396 - 398)*, 2009. *Bioceramics 21*: p. 69-75.
 - [47] Bonfield, W., Biomaterials: Research and Development, in *European White Book on Fundamental Research in Materials Science*. 2000, Max-Planck-Institut Furmetall For Schungstuttgart.

-
- [48] Gomez-Vega, J.M., et al., Aligned bioactive mesoporous silica coatings for implants. *Journal of materials science. Materials in medicine*, 2001. 12(10-12): p. 923-927.
 - [49] Gomez-Vega, J.M., et al., Spin casted mesoporous silica coatings for medical applications. *Thin-Solid Films*, 2001. 398-399: p. 615-620.
 - [50] Thian, E.H., J. Best, SM. Barber, ZH. Bonfield, W, Novel silicon-doped hydroxyapatite (Si-HA) for biomedical coatings: *An in vitro study using acellular simulated body fluid*. 2006.
 - [51] Pramatarova, L., et al., Porous silicon as a substrate for hydroxyapatite growth. *Vacuum*, 2004. 76(2-3): p. 135-138.
 - [52] Shaoqiang, C., et al., Hydroxyapatite coating on porous silicon substrate obtained by precipitation process. *Applied Surface Science*, 2004. 230 (1-4): p. 418-424.
 - [53] Gibson, I.R., et al., Enhanced in vitro cell activity and surface apatite layer formation on novel silicon-substituted hydroxyapatites 2009.
 - [54] Sánchez, A., et al., Nano-hydroxyapatite colloid suspension coated on chemically modified porous silicon by cathodic bias: a suitable surface for cell culture. *physica status solidi (c)*, 2011. 8(6): p. 1898-1902.
 - [55] Kim, Y.H., et al., Preparation of porous Si-incorporated hydroxyapatite. *Current Applied Physics*, 2005. 5(5): p. 538-541.
 - [56] Niu, Y., X. Liu, and C. Ding, Vacuum-plasma-sprayed silicon coatings for biomedical application. *Materials Science and Engineering: C*, 2008. 28(7): p. 1132-1137.
 - [57] Porter, A.E., et al., The structure of the bond between bone and porous silicon-substituted hydroxyapatite bioceramic implants. *Journal of biomedical materials research. Part A*, 2006. 78(1): p. 25-33.
 - [58] Li, D.-H., et al., Synthesized silicon-substituted hydroxyapatite coating on titanium substrate by electrochemical deposition. *Journal of materials science. Materials in medicine*, 2011. 22(5): p. 1205-1211.
 - [59] Zhang, E. and C. Zou, Porous titanium and silicon-substituted hydroxyapatite biomodification prepared by a biomimetic process: Characterization and in vivo evaluation. *Acta Biomaterialia*, 2009. 5(5): p. 1732-1741.
 - [60] Zhang, Z., et al., Osteoblast-like cell adhesion on porous silicon-incorporated TiO₂ coating prepared by micro-arc oxidation. *Journal of biomedical materials research. Part B, Applied biomaterials*, 2011. 97(2): p. 224-234.

- [61] Prestidge, C.A., et al., Loading and release of a model protein from porous silicon powders. *physica status solidi (a)*, 2007. 204(10): p. 3361-3366.
- [62] Salonen, J., et al., Mesoporous silicon microparticles for oral drug delivery: loading and release of five model drugs. *Journal of controlled release : official journal of the Controlled Release Society*, 2005. 108 (2-3): p. 362-374.
- [63] Lee, C., et al., The properties of porous silicon as a therapeutic agent via the new photodynamic therapy. *Journal of Materials Chemistry*, 2007. 17(25).
- [64] Tasciotti, E., et al., Mesoporous silicon particles as a multistage delivery system for imaging and therapeutic applications. *Nat. Nano*, 2008. 3(3): p. 151-157.
- [65] Sapelkin, A.V., et al., Interaction of B50 rat hippocampal cells with stain-etched porous silicon. *Biomaterials*, 2006. 27(6): p. 842-846.
- [66] Zhang, J., et al., In situ loading of basic fibroblast growth factor within porous silica nanoparticles for a prolonged release. *Nanoscale research letters*, 2009. 4(11): p. 1297-1302.
- [67] Chadwick, E., O. Clarkin, and D.A. Tanner, Hydroxyapatite formation on metallurgical grade nanoporous silicon particles. *Journal of Materials Science*, 2010. 45(23): p. 6562-6568.